PAPER

Nitrene-functionalized ruthenium nanoparticles†

Xiongwu Kang, Yang Song and Shaowei Chen*

Ruthenium nanoparticles protected by ruthenium–nitrene π bonds were prepared by refluxing "bare" ruthenium colloids (2.12 ± 0.72 nm in diameter) and 4-dodecylbenezenesulfonyl azide in *sec*-butylbenzene. Thermogravimetric analysis (TGA) of the resulting nanoparticles showed that on average there were about 84.1 ligands on the nanoparticle surface. XPS studies showed a 1 : 1 atomic ratio between nitrogen and sulfur, consistent with the formation of nitrene fragments by the thermal decomposition of the azide precursors. In addition, the binding energies of Ru3d and N1s electrons suggested a covalent nature of the Ru=N interfacial linkage which appeared in FTIR measurements with a vibrational band at 1246 cm^{-1}. Because of such conjugated bonding interactions, extensive intraparticle charge delocalization occurred, and the nanoparticle-bound nitrene moieties behaved analogously to azo derivatives, as manifested in UV-vis and fluorescence measurements. Further testimony of the formation of Ru=N interfacial linkages was highlighted in the unique reactivity of the nanoparticles with alkenes by imido transfer, which was evidenced in spectroscopic and electrochemical studies.

Introduction

Organically capped metal nanoparticles have been attracting intensive research interest from both fundamental and technological perspectives, largely because these nanomaterials show unique optical and electronic properties that can be readily regulated by the chemical nature of the core metals, the organic ligands as well as the metal–ligand interfacial bonding interactions.[1] Among these, the last factor has been the central subject of a series of recent studies, with nanoparticles passivated by metal–carbon covalent linkages.[2–8] Note that whereas mercapto derivatives have been used as the ligands of choice for surface passivation of metal nanoparticles because of the strong affinity of thiol groups to transition metals, recent studies have shown that other metal–ligand bonding chemistry may be exploited for further and more deliberate functionalization of the nanoparticles, leading to the emergence of unprecedented optical and electronic properties.[2–8] For instance, intraparticle charge delocalization has been observed with functional groups bound onto ruthenium nanoparticle surfaces by ruthenium–carbene (Ru=C) π bonds, ruthenium–acetylide (Ru–C≡), or ruthenium–vinylidene (Ru=C=CH–) linkages,[3,7,8] where the electrochemical and spectroscopic characteristics are analogous to those of their dimeric counterparts with a conjugated spacer, thanks to the conducting metal cores.

Within this experimental context, one may ask, is it possible to extend the metal–ligand interfacial bonding interactions to other functional moieties? One intriguing candidate is nitrene derivatives. Note that metal–nitrene (M=N) bonds have been proposed and/or recognized in a variety of organometallic complexes that are involved in bond-activation reactions (*e.g.*, C–H bond activation, nitrene-exchange or -transfer reactions, *etc.*), where the unique reactivity is attributed to the high polarizability of the M=N bonds.[9–11] The nitrene moieties can be produced effectively by thermal or photo-decomposition of the corresponding azide compounds.[12–15] For instance, Leinonen *et al.*[15] reported that *p*-toluenesulfonyl, methylsulfonyl and trimethylsilyl nitrene might be derived by microwave thermal activation from the corresponding azides and covalently grafted onto the surface of single-walled carbon nanotubes. Furthermore, it was found that whereas an appreciable amount of sulfur dioxide might be produced in the decomposition of aliphatic sulfonyl azides, very little is observed with aryl sulfonyl azides which typically decompose in a clean, first-order reaction. This suggests that the stability of the nitrene radicals might be markedly enhanced by using aryl precursors.[12] In metal–azido complexes, thermal- or light-induced decomposition has also been exploited to produce metal–nitrene bonds. For instance, Meyer and co-workers[16] reported that controlled decomposition of ruthenium(III) azido(bis-2,2′-bipyridine) complexes led to the formation of the corresponding ruthenium–nitrene compounds. It is generally believed that the nitrene group is stabilized by the dπ (metal) → pπ (nitrene) back-bonding interactions that involve both σ and π components.[16]

Department of Chemistry and Biochemistry, University of California, 1156 High Street, Santa Cruz, California 95064, USA. E-mail: shaowei@ucsc. edu; Fax: +1 (831) 459-2935; Tel: +1 (831) 459-5841

† Electronic supplementary information (ESI) available: Representative TEM micrograph and core size histogram of Ru=N nanoparticles, NMR spectra of the Ru=N and Ru=N(Fc) nanoparticles and monomeric ligands. See DOI: 10.1039/c2jm33783e

19250 | *J. Mater. Chem.*, 2012, **22**, 19250–19257

This journal is © The Royal Society of Chemistry 2012

Thus, in this study, using an aryl sulfonyl azide ligand as the precursor, we demonstrated that upon thermal decomposition, the resulting nitrene radicals could be readily bound onto "bare" ruthenium colloid surfaces forming ruthenium-nitrene π bonds. The conjugated interfacial bonding interactions led to apparent intraparticle charge delocalization, and the nanoparticle-bound nitrene moieties behaved analogously to azo derivatives, as manifested in a variety of spectroscopic measurements. Interestingly, the resulting nanoparticles also exhibited apparent activity in imido transfer with alkene derivatives, as highlighted in the cyclic addition of vinyl ferrocene to the Ru=N interfacial linkages by spectroscopic and electrochemical measurements. To the best of our knowledge, this is the first report ever on the functionalization of transition-metal nanoparticles with metal–nitrene π bonds.

Experimental section

Chemicals

Ruthenium chloride (RuCl$_3$, 99+%, ACROS), 1,2-propanediol (ACROS), sodium acetate trihydrate (NaOAc·3H$_2$O, MC&B), vinyl ferrocene (97%, Sigma-Aldrich), tetra-n-butylammonium nitrate (TBANO$_3$, ≥99%, Sigma-Aldrich), and 4-dodecylbenzenesulfonyl azide (Aldrich) were used as received. All solvents were obtained from typical commercial sources and used without further treatment. Water was supplied by a Barnstead Nanopure water system (18.3 MΩ cm).

Ruthenium nanoparticles

The synthetic procedure of organically capped ruthenium nanoparticles involved two major steps (Scheme 1). The first was the preparation of "bare" ruthenium colloids by thermolysis of RuCl$_3$ in 1,2-propanediol, as detailed previously.[17,18] Briefly, 0.14 mmol of RuCl$_3$ and 80 mg of NaOAc were co-dissolved in 100 mL of 1,2-propanediol and the mixed solution was heated to 165 °C and thermally refluxed for 30 min under vigorous stirring. The solution displayed a dark brown colour, signifying the formation of ruthenium colloids, which exhibited an average core diameter of 2.12 ± 0.72 nm, as determined by transmission electron microscopic (TEM) measurements.[17,18] These "bare" colloids were then subject to nitrene functionalization in the second step. Experimentally, when the ruthenium colloid solution was cooled down to 60 °C, 0.52 mmol of 4-dodecylbenzenesulfonyl azide in 20 mL of sec-butylbenzene was added into the

solution. After vigorous mixing for 1 h, the ruthenium nanoparticles were extracted into the sec-butylbenzene phase, as manifested by the appearance of a dark brown colour and a colourless propanediol phase. The sec-butylbenzene portion was then collected and underwent a second thermal refluxing at 165 °C for 24 h, where nitrene radicals were produced from the thermolysis of the azide compounds and bound onto the Ru nanoparticle surface.[12] The solution was allowed to cool down naturally to room temperature and the solvents were removed by rotary evaporation. The solids were then rinsed with a copious amount of methanol to remove excessive ligands. The resulting nanoparticles were denoted as Ru=N, which were stable under ambient conditions and readily dispersible in various apolar solvents such as methylene chloride, chloroform and toluene, but not in polar solvents (*e.g.*, alcohols, acetone, *etc.*). The nanoparticle core size remained practically unchanged, as estimated by TEM measurements, 2.06 ± 0.31 nm (Fig. S1 in the ESI†).

Ferrocenyl functionalization of the Ru=N nanoparticles was carried out by mixing the Ru=N nanoparticles with a calculated amount of vinyl ferrocene in CH$_2$Cl$_2$ under magnetic stirring for three days (Scheme 1). The solution was then dried by rotary evaporation and the remaining solids were rinsed extensively by methanol to remove excessive ligands, affording Ru=N nanoparticles with multiple copies of ferrocenyl moieties. The resulting nanoparticles were denoted as Ru=N(Fc).

As a control experiment, carbene-stabilized ruthenium nanoparticles were prepared by following a similar procedure, as described previously.[17] Briefly, after the "bare" Ru colloids were prepared thermolytically, a toluene solution with a calculated amount of octyl diazoacetate (ODA) was added to the colloid solution, where carbene fragments were self-assembled onto the Ru nanoparticle surface forming Ru–carbene (Ru=C) π bonds (and concurrently releasing nitrogen). The purified nanoparticles were referred to as Ru=C8.

Characterization

^{1}H and ^{13}C NMR spectroscopic measurements were carried out by using concentrated solutions of the nanoparticles in CDCl$_3$ or CD$_2$Cl$_2$ with a Varian Unity 500 MHz NMR spectrometer. UV-vis spectroscopic studies were performed with an ATI Unicam UV4 spectrometer using a 1 cm quartz cuvette at a resolution of 2 nm. Photoluminescence characteristics were examined with a PTI fluorospectrometer. FTIR measurements were carried out with a Perkin–Elmer FTIR spectrometer (Spectrum One,
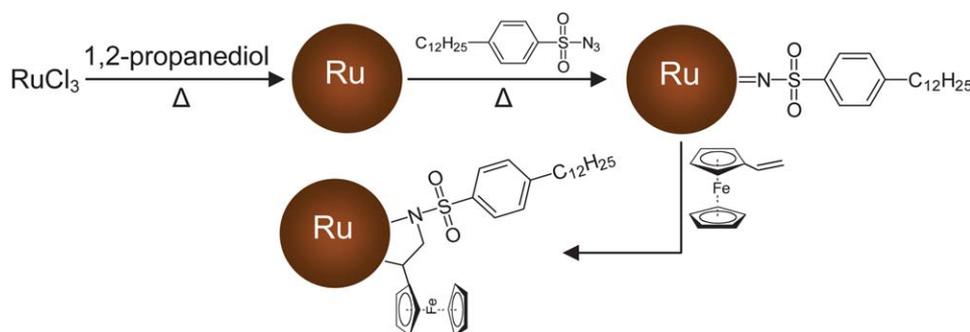
Scheme 1

spectral resolution 4 cm^{-1}); the samples were prepared by casting the particle solutions onto a NaCl disk. Thermogravimetric analysis (TGA) was performed with a Perkin-Elmer Pyris 1 instrument at a heating rate of 10 °C min^{-1} under a nitrogen atmosphere. X-ray photoelectron spectra (XPS) were recorded with a PHI 5400/XPS instrument equipped with an Al Kα source operated at 350 W and at 10^{-9} Torr. The spectra were charge-referenced to the Au4f$_{7/2}$ peak (83.8 eV) of sputtered gold.

Electrochemistry

Voltammetric measurements were carried out with a CHI 440 electrochemical workstation. A polycrystalline gold disk electrode with a surface area of 0.43 mm^2 (sealed in glass tubing) was used as the working electrode. A Ag/AgCl wire and a Pt coil were used as the (quasi)reference and counter electrodes, respectively. The gold electrode was first polished with alumina slurries of 0.05 μm and then cleansed by sonication in 0.1 M HNO$_3$, H$_2$SO$_4$, and Nanopure water successively. The nanoparticles were dispersed in CH$_2$Cl$_2$ at a concentration of 4.2 mg mL^{-1} with 0.1 M TBANO$_3$.

Results and discussion

The bonding interactions between the nitrene moieties and the ruthenium nanoparticles were first examined by XPS measurements. Fig. 1 (A) depicts the survey spectrum of Ru=N nanoparticles where the key elements of the nanoparticles can be clearly identified, Ru, N, S, O and C. In addition, the high-resolution scans of the Ru3d, N1s and S2p electrons are included in panels (B) to (D), respectively. From panel (B), one can see that the Ru 3d$_{5/2}$ and 3d$_{3/2}$ electrons of the Ru=N nanoparticles exhibited a binding energy of 280.3 eV and 284.4 eV (note that the latter also overlaps with the C1s electrons[19–23]), respectively, only ~0.1 eV more positive than that observed with metallic ruthenium (which typically shows two peaks at 280.2 eV and 284.3 eV for the 3d$_{5/2}$ and 3d$_{3/2}$ electrons, respectively[24,25]). This suggests little charge transfer between the ruthenium metal cores and the nitrene moieties, consistent with the binding energy of the N1s electrons, as depicted in panel (C). It can be seen that deconvolution of the N1s spectrum yields only one peak (398.8 eV), as highlighted by the good agreement between the experimental data (black curve) and the curve fit (red curve), indicating that the nitrogen elements are involved in only one chemical state. This is in sharp contrast to the azide moieties (–N=N+=N–) of the monomeric ligands where the nitrogen 1s electrons exhibit two distinctly different binding energies at ca. 402.1 eV and 405.9 eV at an atomic ratio of 2 : 1, with the smaller peak corresponding to the relatively electron-deficient middle nitrogen atom (Fig. S2†).[26] Furthermore, such a binding energy of 398.8 eV for the N1s electrons in Ru=N nanoparticles is consistent with those observed with pyridine-like nitrogen embedded within a graphene matrix (398.2 eV)[27,28] as well as sp^2 nitrogen in metal-coordinated porphyrin complexes (398.2–398.5 eV),[29] signifying the covalent and conjugated nature of the Ru=N bonding interactions.

The S2p electrons can be identified with a peak at 167.8 eV, as manifested in panel (D). This is 1.0 eV lower than that reported in the literature for sulfonamide moieties (–SO$_2$N–, 168.8 eV),[30] and 1.7 eV lower than that observed with the azide monomers

(Fig. S2†), possibly because of the highly delocalized Ru=N interfacial bonding linkages where extended spilling of core electrons into the ligand shell might occur.[3,8] Significantly, based on the integrated peak areas, the atomic ratio of the S and N elements was estimated to be 1.01 : 1, in sharp contrast to the 1 : 3 ratio that was observed with the azide precursors (Fig. S2†).

Taken together, the XPS data presented above strongly suggest that indeed the azide precursors were thermally decomposed into nitrene fragments,[31–33] which were then covalently bound onto the ruthenium nanoparticle surface forming Ru=N π bonds (Scheme 1). This was further confirmed in ^{1}H and ^{13}C NMR measurements (Fig. S3†), where the spectral features of the nanoparticles were all markedly broadened, as compared with those of the monomeric ligands, indicating that the ligands were indeed bound onto the nanoparticle surface and there were no excess free ligands, consistent with earlier studies of organically capped nanoparticles.[34]

The molecular structures of the nitrene fragments on the nanoparticle surface were further investigated by FTIR measurements. Fig. 2 displays the FTIR spectra of the monomeric 4-dodecylbenzenesulfonyl azide ligands (black curve) and the Ru=N nanoparticles (red curve). It can be seen that the phenyl =C–H stretching vibrations at ca. 3063 and 3028 cm^{-1} as well as the ring skeleton vibrations between 1400 cm^{-1} and 1600 cm^{-1} can be clearly identified in both the azide monomers and nanoparticles. In addition, three vibrational bands can be seen with the azide monomers at 1923 cm^{-1}, 1801 cm^{-1} and 1667 cm^{-1}. These may be assigned to the overtone and/or combination of the out-of-plane ring C–H deformations which for disubstituted benzene typically appear between 800 cm^{-1} and 1000 cm^{-1};[35] in contrast, only two peaks are observed with the Ru=N nanoparticles at 1979 cm^{-1} and 1719 cm^{-1}, likely because the ligands are tightly packed on the nanoparticle surface that sterically restricts the ring C–H deformations. In fact, the antisymmetric (d$^-$) and symmetric (d$^+$) stretches of the ligand methylene (CH$_2$) groups of the dodecyl component exhibited a red-shift from 2929 cm^{-1} and 2858 cm^{-1} for the monomeric azide to 2925 cm^{-1} and 2856 cm^{-1} for the Ru=N nanoparticles, indicating enhanced ordering of the ligands when bound on the Ru particle surface as compared with the monomeric counterparts.[7]

The tight packing of the nitrene fragments on the nanoparticle surface may also account for the discrepancy of other vibrational characteristics. For instance, the ring breathing (δ$_{ring}$) at ca. 752 cm^{-1} was substantially weaker with the Ru=N nanoparticles than with the monomeric azide. The symmetrical and asymmetrical stretches of the sulfonyl (–SO$_2$–) moieties can be identified at 1171 cm^{-1} and 1309 cm^{-1}, respectively, for the monomeric azide.[36] Yet, for the nanoparticle sample, their intensities diminished drastically, again likely due to the steric restriction at the core–ligand interface.

The most striking difference between the azide monomers and the Ru=N nanoparticles, however, lies in the stretching vibrations of the azide (N$_3$) moieties. For the monomers, the asymmetrical vibrations of N$_3$ can be clearly identified by two prominent peaks at 2127 cm^{-1} and 2384 cm^{-1}.[36] Yet both of these vanished completely in the nanoparticle samples, consistent with the efficient decomposition of the azide ligands forming nitrene radicals. Note that the azide symmetrical vibration,
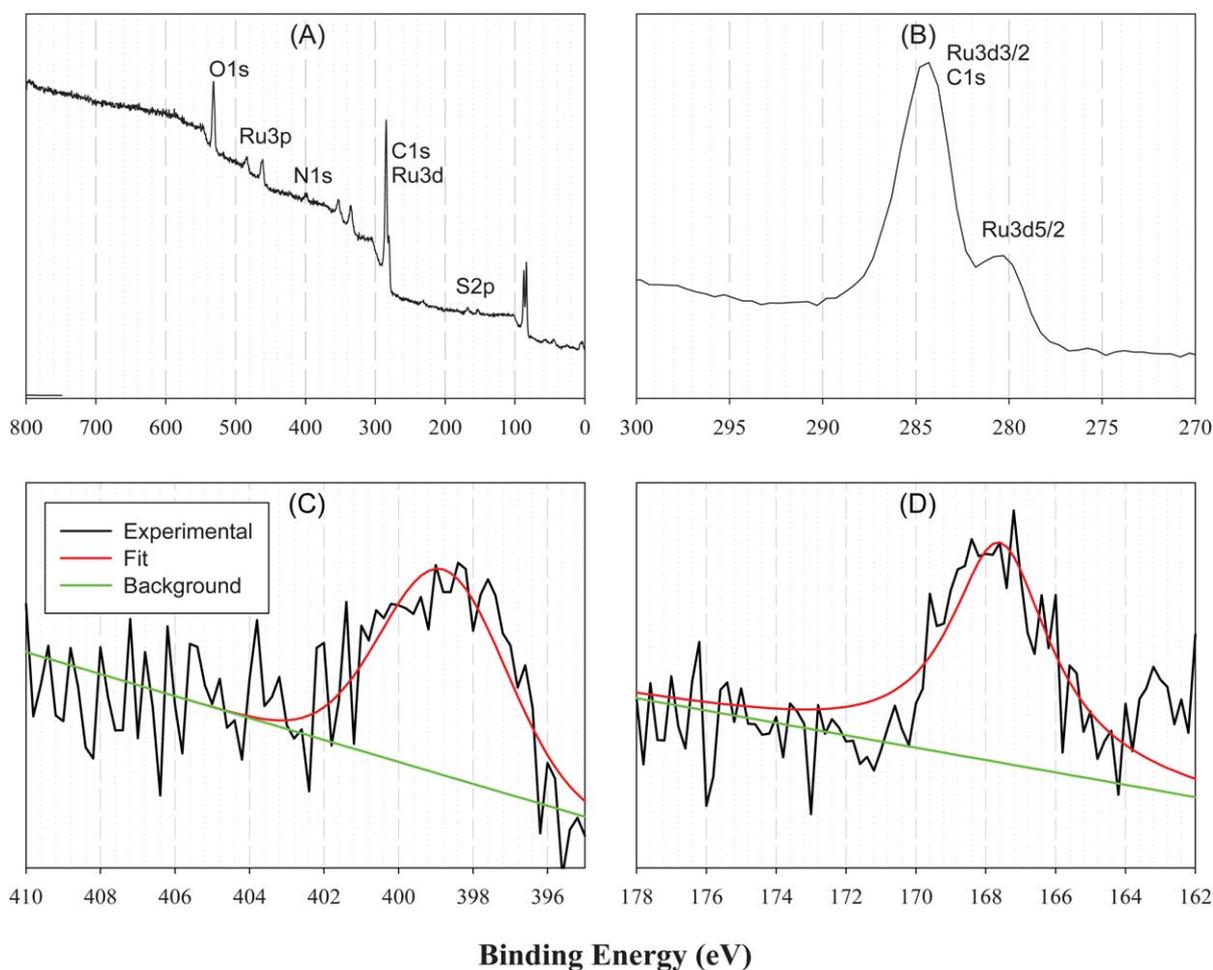
Fig. 1 (A) Full XPS survey spectrum of Ru=N nanoparticles where all key elements of the nanoparticles are identified, and high-resolution scans of (B) Ru3d, (C) N1s, and (D) S2p electrons. In panels (C) and (D), black curves are the experimental data, red curves are the fit, and green curves are the background.

which most likely arises at 1383 cm^{-1}, overlaps with the skeleton stretching of the phenyl ring.[36] Thus, for the monomeric ligands, the peak is very well-defined. Yet, for the Ru=N nanoparticles, one can see a significant diminishment of the peak intensity because of the loss of the azide moiety (Fig. 2).

Then one major question remains. Can the Ru=N bond be resolved in infrared measurements? It should be noted that it remains a challenge to unambiguously identify the spectroscopic signatures of metal–nitrene bonds, although the syntheses of metal–nitrene complexes have been reported in the literature, largely because of the sensitive dependence of the vibrational frequency on the charge state of the metal centers as well as on the substituent groups on the nitrogen atom where coupling with other vibrations within the molecules is possible.[37–39] Of these, the ruthenium–nitrene (Ru=N) π bonds have been shown to appear at frequencies ranging from 900 cm^{-1} to 1300 cm^{-1} in various organometallic complexes.[10,40,41] For instance, Che and co-workers reported the preparation of stable *tert*-butylimido complexes of ruthenium(VI) porphyrins and assigned the IR band at 1232 cm^{-1} to the Ru^{VI}=NBu^t bonding stretch.[42] In another study, they prepared two bis(tosyl)imidoruthenium(VI) porphyrin complexes, Ru^{VI}(tpp)(NTs)$_2$ and Ru^{VI}(oep)(NTs)$_2$,

with tpp = dianion of 5,10,15,20-tetraphenylporphyrin, oep = dianion of 2,3,7,8,12,13,17,18-octaethylporphyrin, and Ts = tosyl, where the asymmetric vibrational band of Ru^{VI} = NTs was observed at 914 cm^{-1} and 900 cm^{-1}, respectively.[40] In light of these earlier results, it is most likely that the new band observed at 1246 cm^{-1} with the nanoparticles (red curve) is due to the Ru=N bonds formed at the metal–ligand interface. As mentioned earlier, the Ru=N bond is stabilized by backbonding interactions of the metal d electrons to nitrogen, and from the XPS studies presented above (Fig. 1), the charge state of ruthenium of the nanoparticles is close to that of neutral metal. Therefore, it is reasonable to conclude that the Ru=N bonding order and hence vibrational frequency of the nanoparticles would be higher than those of the Ru^{VI}=N complexes.

The coverage of nitrene fragments on the nanoparticle surface was then quantified by TGA measurements. Fig. 3 depicts the decrease of the nanoparticle sample weight with temperature (black curve), along with the corresponding first-order derivative (green curve). One can see that the weight loss of the nanoparticle organic components commenced at around 250 °C and ended at around 500 °C, with a total weight loss of 44.2%. Based on the Ru core diameter of 2.06 nm, the number of nitrene fragments on
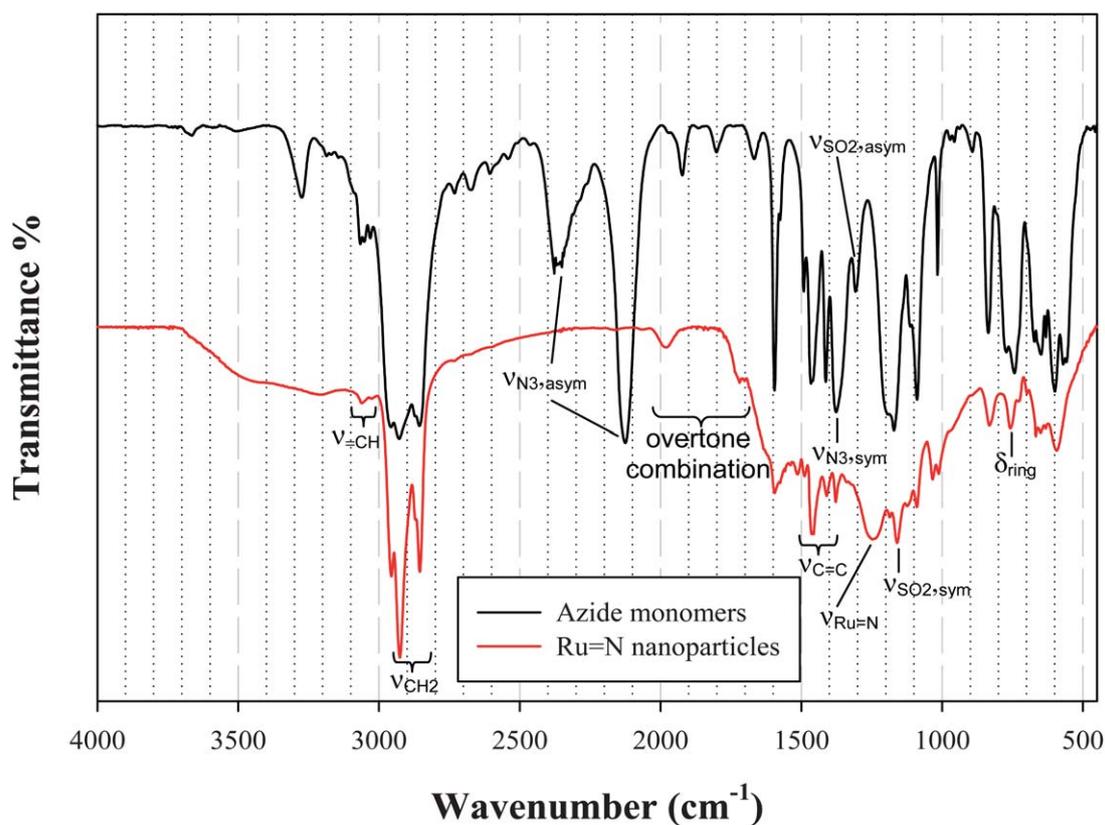
Fig. 2 FTIR spectra of 4-dodecylbenzenesulfonyl azide monomers (black curve) and Ru=N nanoparticles (red curve).
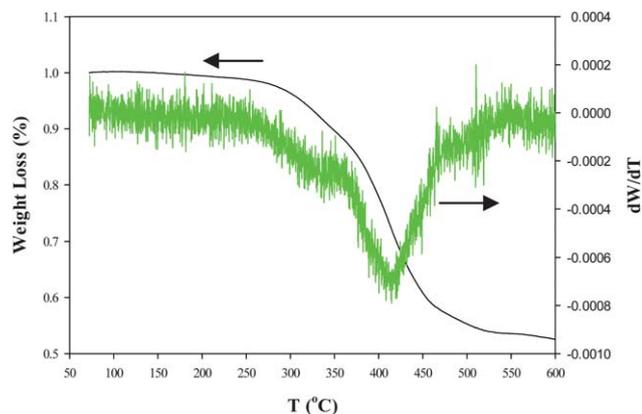

Fig. 3 TGA spectrum (black curve) of Ru=N nanoparticles at a heating rate of 10 °C min^{-1}. The corresponding first-order derivative is also included as the green curve.

the nanoparticle surface can be estimated to be *ca.* 84.1, corresponding to an average footprint of 15.8 Å^2 for one nitrene ligand. This is somewhat greater than that observed with alkyne or alkynide ligands on ruthenium nanoparticles.[43] Furthermore, from the first-order derivative of the TG curve in Fig. 3, it can be seen that the transition temperature of the organic weight loss is around 414 °C. This is more than 100 °C higher than those observed with ruthenium nanoparticles capped by alkyne molecules through ruthenium–vinylidene bonds (<300 °C),[7] suggesting that the ruthenium–nitrene π bonds are substantially

stronger than the ruthenium–carbon π bonds. In fact, the vibrational frequency of the latter was estimated to be 1030 cm^{-1} by Ashkenazi *et al.* in the study of a metallaquinone complex.[44] This is markedly lower than that observed above in the present study for the Ru=N bonds (Fig. 2).

Further studies revealed that the Ru=N nanoparticles exhibited interesting optical properties. Fig. 4 depicts the UV-vis absorption spectra of the azide monomers (black curve), Ru=N nanoparticles (red curve), and Ru=C8 nanoparticles (green curve). Note that the spectra of Ru=N and Ru=C8 nanoparticles were both normalized to their respective absorbance at 300 nm, and their difference is shown as the blue curve. It can be seen that the azide monomers exhibited three absorption peaks at 238 nm, 267 nm and 278 nm. The first peak may be ascribed to the π–π* transition of the phenyl π electrons, whereas the last two peaks are most likely due to the azide moiety.[26] For the Ru=N nanoparticles, in addition to the exponential decay profile that is characteristic of nanosized metal nanoparticles (the so-called Mie scattering),[45] the phenyl absorption peak remained well-defined with a blue-shift to 230 nm, whereas the azide absorption features disappeared, consistent with the decomposition of the azide groups forming nitrene derivatives (*vide ante*). More interestingly, in comparison with the absorption spectrum of the same ruthenium nanoparticles stabilized by carbene fragments (Ru=C8), the Ru=N nanoparticles displayed a new broad absorption band within the range of 340 nm to 650 nm (centered at *ca.* 390 nm), as manifested in the difference spectrum (blue curve). Such
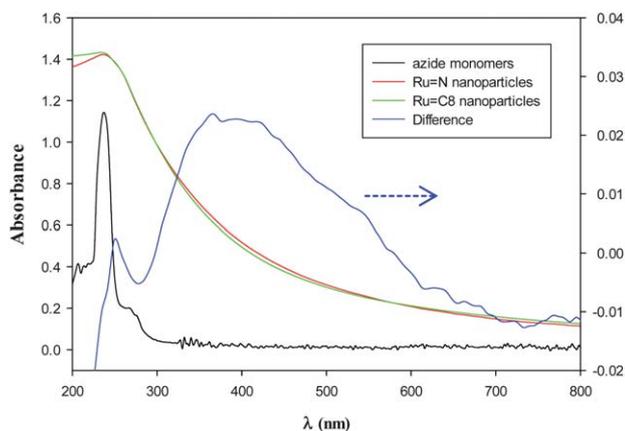
Fig. 4 UV-vis absorption spectra of 4-dodecylbenzenesulfonyl azide monomers (black curve), Ru=N nanoparticles (red curve), and Ru=C8 nanoparticles (green curve) in CH_2Cl_2. The spectra of Ru=N and Ru=C8 nanoparticles were normalized to their respective absorbance at 300 nm and their difference is shown as the blue curve (right axis).

emergence of new electronic energy states with the Ru=N nanoparticles is most likely attributed to intraparticle charge delocalization between the nanoparticle-bound nitrene moieties because of the conjugated Ru=N interfacial bonding interactions, such that the nitrene moieties behave analogously to azo (–N=N–) derivatives. In fact, one may note that 1,2-dialkyldiazenes (RN=NR) have been found to display a prominent absorption band where the peak varied from 340 nm to 380 nm with the chemical structure of the aliphatic substituents.[46,47] Such a behaviour has been observed previously with other fluorophores (*e.g.*, anthracene, pyrene, *etc.*) bound onto the nanoparticle surface by ruthenium–carbene (Ru=C) π bonds.[6]

In fact, the Ru=N nanoparticles exhibited fluorescence characteristics that are similar to those of azoalkanes. The black curves of Fig. 5 show the excitation and emission spectra of the Ru=N nanoparticles, where the excitation peak can be identified
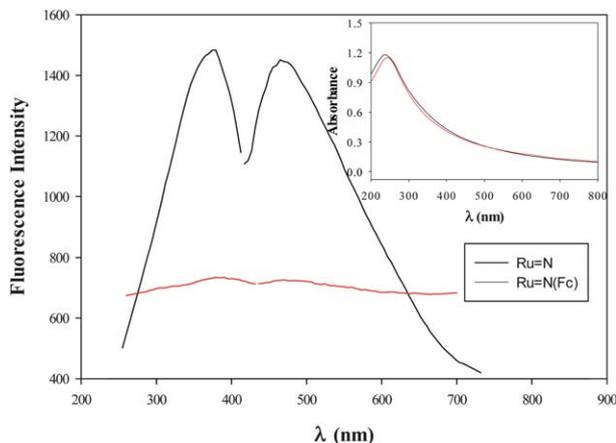
at 375 nm, consistent with the UV-vis spectroscopic measurements (Fig. 4), and the emission peak at 467 nm, in agreement with those of azoalkanes.[48,49] It should be noted that no fluorescence emission was detected with the azide monomers. Thus, the apparent fluorescence of the Ru=N nanoparticles further confirms the effective intraparticle charge delocalization between the particle-bound nitrene moieties that was facilitated by the conjugated Ru=N π bonds, akin to that observed with ruthenium–carbene, –acetylide, or –vinylidene interfacial linkages.[2–8]

The formation of ruthenium–nitrene π bonds at the metal–ligand interface was also manifested by the unique reactivity of the Ru=N nanoparticles with vinyl derivatives, most probably following the imido transfer mechanism that results in the cyclic addition of the vinyl moiety to the Ru=N linkage, as depicted in Scheme 1. Note that imido transfer has been observed with ruthenium–imido complexes for the aziridination of varied arenes such as styrene, norbornene, indene, *etc.*[10] In the present study, we used vinyl ferrocene as the probe molecule to highlight the aziridination properties of the Ru=N nanoparticles. The successful attachment of the ferrocenyl moieties onto the nanoparticle surface was confirmed by varied spectroscopic measurements. Fig. S4† depicts the ^{1}H NMR spectrum of the Ru=N(Fc) nanoparticles. First, one can see that, again, the spectroscopic features of the Ru=N(Fc) nanoparticles were markedly broadened, in comparison with those of the corresponding monomeric ligands. This observation is similar to that of the as-prepared Ru=N nanoparticles (Fig. S3†), where the absence of sharp NMR signals indicates that nanoparticles were free of excessive monomeric ligands and the responses were all due to particle-bound molecules.[3,4,8,17] Second, in contrast to the Ru=N nanoparticles, the Ru=N(Fc) sample exhibited a new (and broad) peak within the range of 3.8 and 4.5 ppm, which is assigned to the particle-bound ferrocenyl protons.[7,8] In addition, in XPS measurements (Fig. S5†), the Ru=N(Fc) nanoparticles also exhibited two peaks at 708.6 eV and 720.7 eV, which are ascribed to the Fe2p electrons.[50]

The particle-bound ferrocenyl moieties were further manifested in electrochemical measurements. Fig. 6 (A) shows the cyclic voltammograms of the Ru=N(Fc) nanoparticles in CH_2Cl_2 with 0.1 M TBANO$_3$ at a potential sweep rate of 200 mV s^{-1}. It can be seen that within the potential range of +0.2 to +0.6 V (*vs.* Ag/AgCl), a pair of prominent peaks appeared with a formal potential ($E^{\circ\prime}$) of +0.40 V, in contrast to the featureless profile of the Ru=N nanoparticles (panel (B)) or the Ru=N
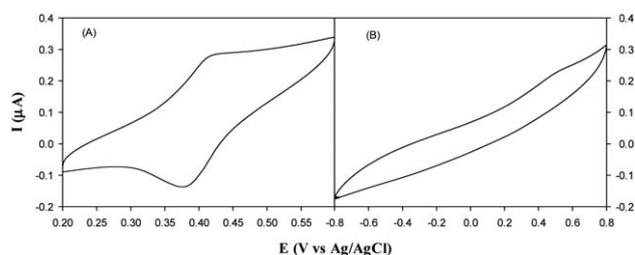

Fig. 5 Excitation and emission spectra of the Ru=N (black curve) and Ru=N(Fc) (red curve) nanoparticles in CH_2Cl_2 with the emission (λ_{em}) and excitation (λ_{ex}) wavelength set at 467 nm and 375 nm, respectively. Inset shows the corresponding (unnormalized) UV-vis absorption spectra.

Fig. 6 Cyclic voltammograms of (A) Ru=N(Fc) and (B) Ru=N nanoparticles both at a concentration of *ca.* 4.2 mg mL^{-1} in CH_2Cl_2 with 0.1 M TBANO$_3$. The working electrode was a gold electrode with a surface area of 0.43 mm^2. The potential sweep rate was 200 mV s^{-1}.

This journal is © The Royal Society of Chemistry 2012

J. Mater. Chem., 2012, **22**, 19250–19257 | 19255

nanoparticles after mixing with ethyl ferrocene for 7 d (not shown). This is ascribed to the 1e reduction–oxidation of nanoparticle-bound ferrocenyl moieties, Fc $\leftrightarrow$ Fc$^+$ + e. The small peak splitting ($\Delta E_p \approx 40$ mV at 200 mV s^{-1}) is consistent with the facile electron-transfer kinetics of ferrocenyl derivatives, although in the Ru=N(Fc) nanoparticles, the ferrocenyl moieties were buried within the hydrophobic ligand shell and the accessibility to counter ions was likely impeded.

Importantly, the fact that only one pair of voltammetric peaks was observed is consistent with the cyclic addition of the vinyl moieties with the Ru=N linkage by imido transfer (Scheme 1) where the ferrocenyl moieties were bound onto the nanoparticle surface by saturated bonds. This is in sharp contrast with our previous studies where olefin metathesis reactions of vinyl ferrocene with carbene-functionalized nanoparticles (e.g., Ru=C8) led to the covalent attachment of the ferrocenyl moieties onto the particle surface by Ru=C π bonds.[8] Consequently, apparent intraparticle charge delocalization occurred, where intervalence transfer between the particle-bound ferrocenyl moieties was manifested in electrochemical studies with two pairs of voltammetric peaks and in near-infrared measurements with a peak emerging at mixed valence, a behaviour consistent with those of Class II compounds.[8]

Furthermore, with the bonding attachment of vinyl ferrocene to the ruthenium-nitrene linkage, the metal–ligand interfacial π bonds are now converted into saturated ones (Scheme 1), leading to effective diminishment of the nanoparticle photoluminescence that arises from the intraparticle charge delocalization between the particle-bound nitrene moieties (vide ante). In fact, as shown in Fig. 5 (red curves), the photoluminescence intensity of the Ru=N(Fc) nanoparticles was significantly weaker than that of the Ru=N nanoparticles (black curves), although the optical density at the excitation wavelength was similar, as depicted in the UV-vis absorption measurements (Fig. 5, inset).

Conclusion

In this study, nitrene fragments generated from the thermolysis of a sulfonyl azide derivative were exploited to functionalize "bare" ruthenium nanoparticles by virtue of the formation of ruthenium–nitrene (Ru=N) π bonds at the metal–ligand interface. XPS measurements of the resulting nanoparticles showed that the atomic ratio between nitrogen and sulfur was about 1 : 1, consistent with the formation of nitrene moieties from the thermal decomposition of azide precursors, and there was little (net) charge transfer between ruthenium and nitrogen, suggesting that the Ru=N linkage was mostly covalent in nature. In fact, UV-vis and photoluminescence measurements indicated that the nanoparticle-bound nitrene moieties behaved analogously to azo (–N=N–) derivatives. This is most probably a result of intraparticle charge delocalization due to the conjugated Ru=N interfacial bonds, which was detected in FTIR measurements with a vibrational band at 1246 cm^{-1}. The formation of Ru=N interfacial bonding linkages was further manifested in the unique reactivity of the nanoparticles towards alkenyl derivatives by imido transfer reactions. With vinyl ferrocene as the probe molecules, the cyclic addition of the vinyl moieties to the Ru=N linkages was highlighted in spectroscopic as well as electrochemical measurements.

In summary, the results presented above demonstrate, for the first time ever, that nitrene chemistry may be readily utilized for the surface functionalization of transition-metal nanoparticles. More importantly, the unique chemical reactivity of the metal–nitrene π bonds may be exploited as an unprecedented platform for further and more complicated manipulation of the optical and electronic properties of the nanoparticle materials. This will be the focus of on-going work.

Acknowledgements

Notes and references

1 S. W. Chen, Electroanalytical Chemistry, ed. A. J. Bard and C. G. Zoski, 2010, 23, 171–210–.
2 W. Chen, L. E. Brown, J. P. Konopelski and S. W. Chen, Chem. Phys. Lett., 2009, 471, 283–285.
3 W. Chen, N. B. Zuckerman, J. W. Lewis, J. P. Konopelski and S. W. Chen, J. Phys. Chem. C, 2009, 113, 16988–16995.
4 W. Chen, N. B. Zuckerman, J. P. Konopelski and S. W. Chen, Anal. Chem., 2010, 82, 461–465.
5 W. Chen, N. B. Zuckerman, X. W. Kang, D. Ghosh, J. P. Konopelski and S. W. Chen, J. Phys. Chem. C, 2010, 114, 18146–18152.
6 W. Chen, S. Pradhan and S. W. Chen, Nanoscale, 2011, 3, 2294–2300.
7 X. W. Kang, N. B. Zuckerman, J. P. Konopelski and S. W. Chen, J. Am. Chem. Soc., 2012, 134, 1412–1415.
8 W. Chen, S. W. Chen, F. Z. Ding, H. B. Wang, L. E. Brown and J. P. Konopelski, J. Am. Chem. Soc., 2008, 130, 12156–12162.
9 I. I. Moiseev, T. A. Stromnova, M. N. Vargaftik, S. T. Orlova, T. V. Chernysheva and I. P. Stolarov, Catal. Today, 1999, 51, 595–602.
10 S. K. Y. Leung, W. M. Tsui, J. S. Huang, C. M. Che, J. L. Liang and N. Y. Zhu, J. Am. Chem. Soc., 2005, 127, 16629–16640.
11 A. F. Heyduk, R. A. Zarkesh and A. I. Nguyen, Inorg. Chem., 2011, 50, 9849–9863.
12 D. S. Breslow, M. F. Sloan, N. R. Newburg and W. B. Renfrow, J. Am. Chem. Soc., 1969, 91, 2273.
13 I. Foch, L. Parkanyi, G. Besenyei, L. I. Simandi and A. Kalman, J. Chem. Soc., Dalton Trans., 1999, 293–299.
14 M. Nomura, A. Kawakita, H. Katsuta, C. Takayama, T. Sugiyama, Y. Yokoyama and M. Kajitani, J. Organomet. Chem., 2003, 681, 180–188.
15 H. Leinonen, J. Rintala, A. Siitonen, M. Lajunen and M. Pettersson, Carbon, 2010, 48, 2425–2434.
16 G. M. Brown, R. W. Callahan and T. J. Meyer, Inorg. Chem., 1975, 14, 1915–1921.
17 W. Chen, J. R. Davies, D. Ghosh, M. C. Tong, J. P. Konopelski and S. W. Chen, Chem. Mater., 2006, 18, 5253–5259.
18 X. W. Kang, W. Chen, N. B. Zuckerman, J. P. Konopelski and S. W. Chen, Langmuir, 2011, 27, 12636–12641.
19 M. Rybachuk and J. M. Bell, Carbon, 2009, 47, 2481–2490.
20 S. Turgeon and R. W. Paynter, Thin Solid Films, 2001, 394, 44–48.
21 U. Dettlaff-Weglikowska, J. M. Benoit, P. W. Chiu, R. Graupner, S. Lebedkin and S. Roth, Curr. Appl. Phys., 2002, 2, 497–501.
22 G. Iucci, V. Carravetta, P. Altamura, M. V. Russo, G. Paolucci, A. Goldoni and G. Polzonetti, Chem. Phys., 2004, 302, 43–52.
23 K. Siegbahn, Philos. Trans. R. Soc., A, 1970, 268, 33.
24 N. Chakroune, G. Viau, S. Ammar, L. Poul, D. Veautier, M. M. Chehimi, C. Mangeney, F. Villain and F. Fievet, Langmuir, 2005, 21, 6788–6796.
25 R. Luque, J. H. Clark, K. Yoshida and P. L. Gai, Chem. Commun., 2009, 5305–5307.

26 E. W. Wollman, D. Kang, C. D. Frisbie, I. M. Lorkovic and M. S. Wrighton, *J. Am. Chem. Soc.*, 1994, **116**, 4395–4404.

27 C. H. Zhang, L. Fu, N. Liu, M. H. Liu, Y. Y. Wang and Z. F. Liu, *Adv. Mater.*, 2011, **23**, 1020–1024.

28 D. Usachov, O. Vilkov, A. Gruneis, D. Haberer, A. Fedorov, V. K. Adamchuk, A. B. Preobrajenski, P. Dudin, A. Barinov, M. Oehzelt, C. Laubschat and D. V. Vyalikh, *Nano Lett.*, 2011, **11**, 5401–5407.

29 D. K. Lavallee, J. Brace and N. Winograd, *Inorg. Chem.*, 1979, **18**, 1776–1780.

30 G. A. Schick and Z. Q. Sun, *Langmuir*, 1994, **10**, 3105–3110.

31 P. G. Cao, K. Xu and J. R. Heath, *J. Am. Chem. Soc.*, 2008, **130**, 14910.

32 C. Radhakrishnan, M. K. F. Lo, M. V. Warrier, M. A. Garcia-Garibay and H. G. Monbouquette, *Langmuir*, 2006, **22**, 5018–5024.

33 J. P. Collman, N. K. Devaraj, T. P. A. Eberspacher and C. E. D. Chidsey, *Langmuir*, 2006, **22**, 2457–2464.

34 M. J. Hostetler, J. E. Wingate, C. J. Zhong, J. E. Harris, R. W. Vachet, M. R. Clark, J. D. Londono, S. J. Green, J. J. Stokes, G. D. Wignall, G. L. Glish, M. D. Porter, N. D. Evans and R. W. Murray, *Langmuir*, 1998, **14**, 17–30.

35 D. H. Whiffen, *Spectrochim. Acta*, 1955, **7**, 253–263.

36 A. Teimouri, A. N. Chermahini, K. Taban and H. A. Dabbagh, *Spectrochim. Acta, Part A*, 2009, **72**, 369–377.

37 M. Ochiai, K. Miyamoto, T. Kaneaki, S. Hayashi and W. Nakanishi, *Science*, 2011, **332**, 448–451.

38 H. M. L. Davies, *Angew. Chem., Int. Ed.*, 2006, **45**, 6422–6425.

39 H. Lebel, O. Leogane, K. Huard and S. Lectard, *Pure Appl. Chem.*, 2006, **78**, 363–375.

40 S. M. Au, W. H. Fung, M. C. Cheng, C. M. Che and S. M. Peng, *Chem. Commun.*, 1997, 1655–1656.

41 S. M. Au, J. S. Huang, W. Y. Yu, W. H. Fung and C. M. Che, *J. Am. Chem. Soc.*, 1999, **121**, 9120–9132.

42 J. S. Huang, C. M. Che and C. K. Poon, *J. Chem. Soc., Chem. Commun.*, 1992, 161–163.

43 X. W. Kang and S. W. Chen, *Nanoscale*, 2012, **4**, 4183–4189.

44 N. Ashkenazi, A. Vigalok, S. Parthiban, Y. Ben-David, L. J. W. Shimon, J. M. L. Martin and D. Milstein, *J. Am. Chem. Soc.*, 2000, **122**, 8797–8798.

45 J. A. Creighton and D. G. Eadon, *J. Chem. Soc., Faraday Trans.*, 1991, **87**, 3881–3891.

46 D. J. Severn and E. M. Kosower, *J. Am. Chem. Soc.*, 1969, **91**, 1710.

47 H. Fliegl, A. Kohn, C. Hattig and R. Ahlrichs, *J. Am. Chem. Soc.*, 2003, **125**, 9821–9827.

48 M. J. Mirbach, M. F. Mirbach, W. R. Cherry, N. J. Turro and P. Engel, *Chem. Phys. Lett.*, 1978, **53**, 266–269.

49 W. M. Nau, *J. Am. Chem. Soc.*, 1998, **120**, 12614–12618.

50 Y. Song, X. W. Kang, N. B. Zuckerman, B. Phebus, J. P. Konopelski and S. W. Chen, *Nanoscale*, 2011, **3**, 1984–1989.

This journal is © The Royal Society of Chemistry 2012

J. Mater. Chem., 2012, **22**, 19250–19257 | 19257